Journal of Hazardous Materials 192 (2011) 150–159

Contents lists available at ScienceDirect

Journal of Hazardous Materials

journal homepage: www.elsevier.com/locate/jhazmat

Highly efficient visible light TiO_2 photocatalyst prepared by sol–gel method at temperatures lower than 300 °C

Desong Wang[a,*], Libin Xiao[a], Qingzhi Luo[a], Xueyan Li[a], Jing An[a], Yandong Duan[b]

[a] School of Sciences, Hebei University of Science and Technology, Shijiazhuang, Hebei 050018, China
[b] College of Chemical and Pharmaceutical Engineering, Hebei University of Science and Technology, Shijiazhuang, Hebei 050018, China

ARTICLE INFO

Article history:
Received 7 December 2010
Received in revised form 27 April 2011
Accepted 30 April 2011
Available online 10 May 2011

Keywords:
Titanium dioxide
Sol–gel method
Carbon self-doping
Visible light photosensitive groups
Photodegradation

ABSTRACT

Highly efficient visible light TiO_2 photocatalyst was prepared by the sol–gel method at lower temperature (≤300 °C), and characterized by X-ray diffraction (XRD), transmission electron microscopy (TEM), Fourier-transform infrared spectroscopy (FTIR), UV–vis diffuse reflectance spectroscopy (UV–vis DRS), X-ray photoelectron spectroscopy (XPS), Raman spectroscopy and differential scanning calorimetry-thermogravimetric analysis (DSC–TGA). The effects of the heat treatment temperature and time of the as-prepared TiO_2 on its visible light photocatalytic activity were investigated by monitoring the degradation of methyl orange solution under visible light irradiation (wavelength ≥ 400 nm). Results show that the as-prepared TiO_2 nanoparticles possess an anatase phase and mesoporous structure with carbon self-doping and visible photosensitive organic groups. The visible light photocatalytic activity of the as-prepared TiO_2 is greatly higher than those of the commercial TiO_2 (P-25) and other visible photocatalysts reported in literature (such as PPy/TiO_2, P3HT/TiO_2, PANI/TiO_2, N–TiO_2 and Fe^{3+}–TiO_2) and its photocatalytic stability is excellent. The reasons for improving the visible light photocatalytic activity of the as-prepared TiO_2 can be explained by carbon self-doping and a large amount of visible photosensitive groups existing in the as-prepared TiO_2. The apparent optical thickness (τ_{app}), local volumetric rate of photo absorption (LVRPA) and kinetic constant (k_T) of the photodegradation system were calculated.

1. Introduction

Nanoparticulate TiO_2 is an important photocatalyst material for the degradation of organic contaminants in water and air because of its high efficiency, inexpensiveness, easy production, photochemical and biological stability, and innocuity to the environment and human beings [1–3]. Consequently, much attention has been paid to investigations on TiO_2 nanoparticles. However, the major drawback of TiO_2 nanoparticles lies in their ineffective use of visible light as irradiation source because the band gap of anatase TiO_2 (3.2 eV) is so wide that it can only absorb and be excited by UV light with wavelength less than 387 nm, which only occupies about 4–6% of the global solar radiation [4–6]. To resolve the above problem, many efforts have been exerted to extend the light absorption of TiO_2 into the visible light region, such as dye sensitization [7–10], transition metals ion doping [11–14], non-metals ion doping [15–21], ion implantation [22], metal deposition [23–26], semiconductor composite [27–30] and conjugated polymer modification [31–34]. In the above mentioned methods, TiO_2 nanoparticles for further modification or modified TiO_2 nanoparticles are usually calcined at higher temperatures (>400 °C), which consumes more energy. So far, only a few papers have reported the visible light photocatalytic activities of TiO_2 prepared at lower temperatures (≤300 °C).

Wang et al. [35] reported a simple and new method for preparing anatase TiO_2 hydrosol with high visible light photocatalytic activity. They first prepared amorphous TiO_2 by adding tetrabutyl titanate dropwise into water and then obtained anatase TiO_2 by processing amorphous TiO_2 with diluted HNO_3 solution at 70 °C. Tseng et al. [36] prepared TiO_2 with a mixed crystal lattice of anatase, brookite and rutile phases by sol–gel process with tetrabutyl orthotitanate and HNO_3 as precursor and catalyst, respectively, at the calcination temperature of 150–600 °C. They studied the visible light photocatalytic activity of the as-prepared TiO_2 with NO_x as model compound, and found that TiO_2 prepared at 200 °C had high visible light photocatalytic activity. They indicated that the carbonaceous species on the surface of TiO_2 may function as sensitizer in improving the visible light photocatalytic activity. Recently, Park et al. [37] reported the visible light photocatalytic activity of TiO_2 prepared by a typical sol–gel method at lower temperatures. They found that the as-prepared TiO_2 samples had high visible light photocatalytic activity, the calcination temperature obviously affected the photocatalytic activity, and the best photocatalytic activity was around 250 °C. The authors attributed the enhancement in visible light photocatalytic activity to carbon self-doping.

* Corresponding author. Tel.: +86 311 8166 9901; fax: +86 311 8166 9901.
E-mail addresses: dswang06@126.com, wangdesong@hebust.edu.cn (D. Wang).

0304-3894/$ – see front matter © 2011 Elsevier B.V. All rights reserved.
doi:10.1016/j.jhazmat.2011.04.110

During studying the visible light photocatalytic activity of TiO_2 nanoparticles prepared by sol–gel method at lower temperatures, we found that heat-treating temperature and heat-treating time greatly influenced the visible light photocatalytic activity of TiO_2. It is difficult to explain the results only using carbonaceous species on the surface of TiO_2 as sensitizer or carbon doping. Therefore, the further detailed investigation should be carried out to interpret the visible light photocatalytic mechanism of TiO_2 nanoparticles prepared at lower temperatures. In the present work, we first prepared TiO_2 nanoparticles at lower temperatures ($\leq$300 °C) by sol–gel method with tetrabutyl titanate and acetic acid as precursor and inhibitor respectively, then characterized them by transmission electron microscopy (TEM), X-ray diffraction (XRD), X-ray photoelectron spectroscopy (XPS), Fourier transform infrared spectroscopy (FTIR), UV–vis diffuse reflectance spectroscopy (UV–vis DRS), and differential scanning calorimetry-thermogravimetric analysis (DSC–TGA), investigated their visible light photocatalytic activity with methyl orange (MO) as model contaminant, calculated the apparent optical thickness(τ_{app}), local volumetric rate of photo absorption (LVRPA) and kinetic constant (k_T) of the photodegradation system, and tried to clarify the reasons for enhancing their visible light photocatalytic activities.

2. Experimental

2.1. Preparation of TiO_2 photocatalyst

Tetrabutyl titanate, absolute ethanol, glacial acetic acid were purchased as A.R. grade chemicals from Beijing Chemical Reagent Company and used without further purification. The preparation of nano-TiO_2 photocatalysts were carried out by sol–gel method as follows: 20 mL tetrabutyl titanate and 4 mL acetic acid were added into 26 mL of absolute ethanol under continuously stirring condition to obtain the solution A. 8 mL deionized water, 12 mL absolute ethanol and 12 mL acetic acid were mixed together to obtain the solution B. Then, the solution B was added dropwise into the solution A under magnetic stirring for 30 min. The obtained solution was sealed and the stirring was continued for another 30 min at room temperature. The resultant gel was aged at room temperature for 24 h and dried in an oven at 100 °C for 36 h. After grinding, the final gels were heat-treated in a furnace at 150 °C, 200 °C, 250 °C, 270 °C and 300 °C for 0.5 h, respectively, or at 270 °C for 5 min, 10 min, 0.5 h, 1 h, 2 h, 10 h, 15 h and 20 h, respectively. The samples were labeled as TiO_2 (x °C, yh) or TiO_2 (x °C, $y$min), where x is the heat-treating temperature, and y is the heat-treating time.

According to the preparation method reported in literature [16,31–33,38], the TiO_2 samples modified by poly(3-hexylthiophene), polyaniline and polypyrrole, or doped by nitrogen and ferric ion were prepared under the optimal conditions. The samples were labeled as P3HT/TiO_2, PANI/TiO_2, PPy/TiO_2, N–$TiO_2$and Fe^{3+}–TiO_2.

2.2. Characterization

The crystal structure of the samples was characterized by X-ray diffractometer (XRD, Rigaku D/MAX2500PC, Japan) with Cu Kα radiation (λ = 1.54056 Å) as X-ray source, operated at 40 kV and 100 mA in the range of 2θ = 10–90°. Crystallite size of anatase TiO_2 can be calculated from the line broadening by Scherrer's formula.

The Brunauer–Emmett–Teller (BET) specific surface area and pore's size measurements were performed by a NOVA 2000 surface area analyzer (Quantachrome, America) with nitrogen as an adsorptive gas.

TiO_2 morphology was studied using transmission electron microscopy (TEM, G2F20, Tecnai Co., Holland) with an accelerating voltage of 200 kV. The TEM samples were prepared by dispersing TiO_2 nanoparticles in ethanol and then dropping the suspension on carbon–copper grids.

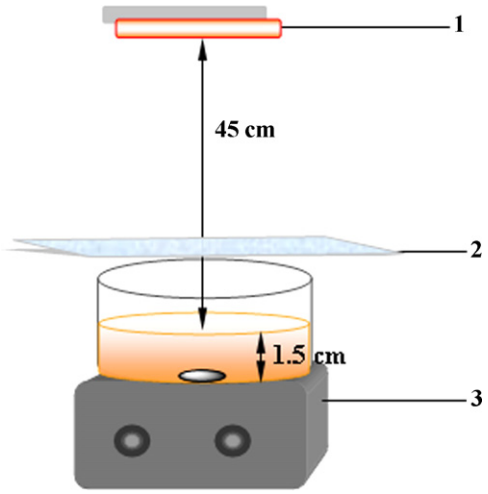

Fig. 1. Scheme of the experimental setup for MO photodegradation. 1— Halogen lamp (300 W); 2— Cutoff filter (400 nm); 3— Magnetic stirrer.

UV–visible diffuse reflectance spectroscopy (UV–vis DRS) was carried out on a Cary 100 Scan UV–vis system (Varian Co., USA) equipped with an integrating sphere attachment over a range of 200–800 nm. Integrating sphere USRS-99-010 was employed as a reflectance standard.

Fourier-transform infrared spectra (FTIR) of the samples were recorded on a Prestige-21 spectrometer (Shimadzu Co., Japan) in the range of 400–4000 cm^{-1} with KBr as the reference sample. Measurements were performed in the transmission mode with spectroscopic grade KBr pellets for all the powders.

Raman spectra were obtained with a Nicolet 6700 Raman microspectrometer at the resolution of 2 cm^{-1} using the 514.5 nm line of an Ar ion laser as the excitation. The accelerating voltage of 30 kV and emission current of 30 mA were used.

X-ray photoelectron spectroscopy (XPS) measurements were performed with the PHI 5000 C ESCA System with Al Kα radiation ($h\nu$ = 1486.6 eV). The X-ray anode was run at 250 W and the high voltage was kept at 15.0 kV with a detection angle of 54°.

DSC–TGA analyses were performed on an STD-2960 thermal analyzer (TA Instruments, America) under a N_2 atmosphere and a heating rate of 10 °C min^{-1}.

2.3. Photocatalytic activity test

The photocatalytic activities were evaluated by the degradation of MO in an aqueous solution under visible light (>400 nm) or sunlight irradiation. The scheme of experimental setup for MO photodegradation is displayed in Fig. 1. The visible light was obtained using a 300 W halogen lamp (Philips Electronics N.V. Netherlands) with a 400 nm cutoff filter to ensure the desired irradiation light. The aqueous solution of MO (100 mL, 10 mg L^{-1}) was placed in a vessel, and 0.1 g of nano-TiO_2 photocatalyst (as-prepared TiO_2, P-25, PPy/TiO_2, PANI/TiO_2, P3HT/TiO_2, N–TiO_2 or Fe^{3+}–TiO_2) was added into the above solution. The selection of TiO_2 concentration was based on the apparent optical thickness of the investigated suspension suggested by Li Puma et al. [39–41]. The reactor was open to air to ensure enough oxygen into the reaction suspensions. The distance between the lamp and the surface of the suspensions was about 45 cm. Prior to irradiation, the suspensions were magnetically stirred in the dark for 60 min to establish an adsorption–desorption equilibrium. At certain time

Table 1
Specific surface area, average size and band gap of TiO_2 heat-treated at 270 °C for different time.

Sample	Specific surface area ($m^2\,g^{-1}$)	Average size (nm)	Band gap (eV)
TiO_2(270 °C, 5 min)	274.4	8.5	3.05
TiO_2(270 °C, 0.5 h)	255.4	9.0	2.79
TiO_2(270 °C, 1 h)	253.1	9.4	2.79
TiO_2(270 °C, 2 h)	243.8	9.8	2.90
TiO_2(270 °C, 10 h)	222.8	10.1	3.08
TiO_2(270 °C, 15 h)	203.2	11.2	3.12
TiO_2(270 °C, 20 h)	196.3	11.4	3.14
P-25	48.2	28.6	3.20

intervals, 3 mL aliquots were sampled and centrifuged to remove the nanoparticles. The filtrates were analyzed by recording variations of absorbancy at the maximum absorption band (464 nm for MO) using an SP-723 Visible spectrophotometer (Shanghai Spectrum Instruments Co., Ltd.). The concentration of MO was calculated using a calibration curve. c_0 and c are the concentrations of MO solutions before and after irradiation, respectively. The reactions were carried out at natural pH conditions.

The photocatalytic activity tests of TiO_2(270 °C, 0.5 h) and the commercial TiO_2(P-25, Degussa Corp.) at different concentrations of 1 g L^{-1}, 0.5 g L^{-1} and 0.2 g L^{-1} under sunlight irradiation were simultaneously carried out in Shijiazhuang, Hebei Province, China at 11:00–12:00 am, 9 April 2011.

3. Results and discussion

3.1. Characterization of as-prepared TiO_2 nanoparticles

3.1.1. TEM and N_2 sorption analysis

The size and morphology of TiO_2(270 °C, 0.5 h) nanoparticles were analyzed by TEM measurements. Fig. 2(a) shows that the as-prepared TiO_2 has a mesoporous structure, and the sizes of the mesopores which possess a long-range disordered structure are about 2–3 nm. Fig. 2(b) indicates that the mean size of TiO_2(270 °C, 0.5 h) nanoparticles is about 8 nm. Although the nanoparticles are agglomerated to some degree, their grain boundaries are distinguishable. Lattice images of the nanoparticles are clearly observed, indicating that these nanoparticles have high crystallinity. The parallel fringe spacing of the nanoparticles is estimated to be 0.35 nm, corresponding to (1 0 1) plane of anatase TiO_2, indicating that this plane is the preferential growth direction of the nanocrystal.

Fig. 3(a) and (b) presents the nitrogen adsorption isotherm and DFT differential pore volume distribution of TiO_2(270 °C, 0.5 h), respectively. The isotherm is a typical IV isotherm (IUPAC, 1985) with a H2 hysteresis loop, which is a typical characteristic of mesoporous materials [42]. A steep rise in the desorption branch is observed at relative pressures of 0.4–0.7, suggesting that the pore distribution is extremely narrow. The Barrett–Joyner–Halenda analysis yields a corresponding peak at the pore diameter of 3.1 nm, which is agreeable with the TEM result. The BET specific surface areas of the as-prepared TiO_2 investigated in this work are in the range of 196.3–289.7 $m^2\,g^{-1}$ by BET method (Tables 1 and 2).

3.1.2. XRD

The XRD spectra of the as-prepared TiO_2 are shown in Fig. 4(a) and (b). The peaks at 25.42°, 37.96° and 48.12° are attributed to the (1 0 1), (0 0 4), (2 0 0) reflections of anatase TiO_2, respectively, slightly shift when compared with those of neat TiO_2 calcined at 500 °C for 2 h (25.3°, 37.8° and 48.1°), indicating that Ti might be replaced by C in the as-prepared TiO_2. The characteristic peaks for rutile and brookite TiO_2 are not observed, revealing that the rutile and brookite phases do not exist in the as-prepared TiO_2.

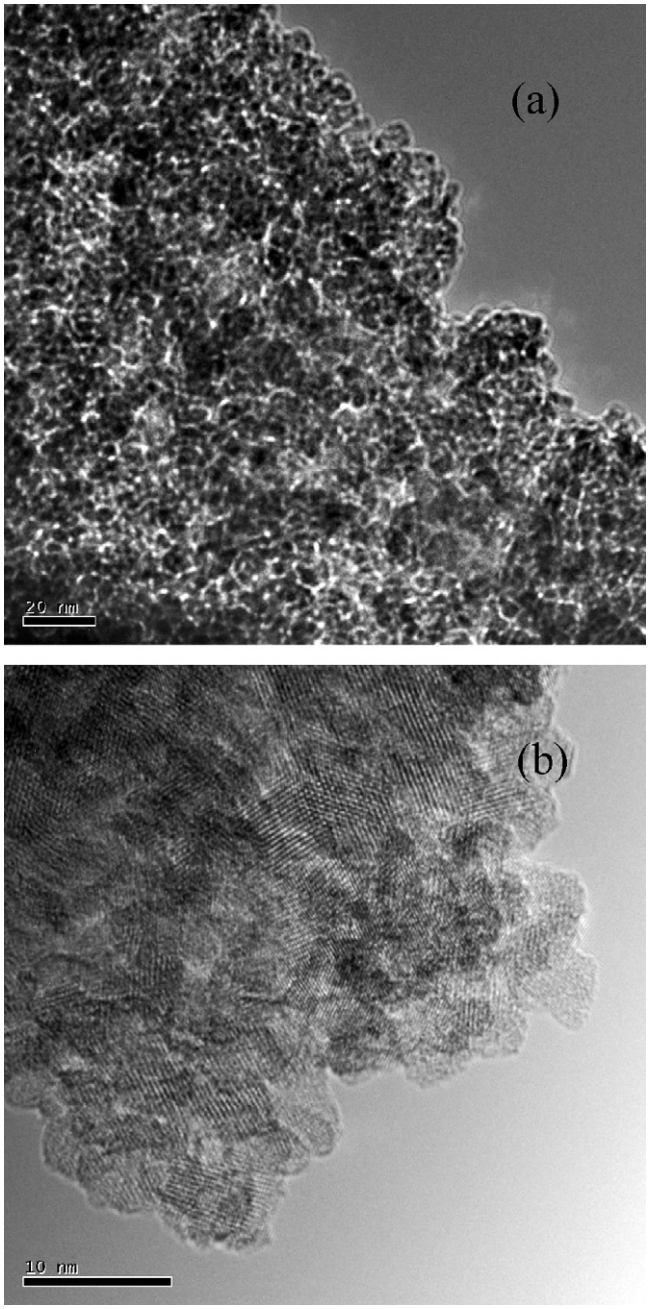

Fig. 2. TEM images of TiO_2(270 °C, 0.5 h) (a) and HRTEM image of TiO_2(270 °C, 0.5 h) (b).

The relatively broad peaks of the XRD patterns imply the small size of the anatase crystals. The mean sizes of the as-prepared TiO_2 nanoparticles, calculated by Scherrer's formula, are in the range of 8.5–11.4 nm (Table 1) for the samples heat-treated at 270 °C for dif-

Table 2
Specific surface area, average size and band gap of TiO_2 heat-treated at different temperature for 0.5 h.

Sample	Specific surface area ($m^2\,g^{-1}$)	Average size (nm)	Band gap (eV)
TiO_2(150 °C, 0.5 h)	289.7	8.2	3.07
TiO_2(200 °C, 0.5 h)	286.4	8.2	3.07
TiO_2(250 °C, 0.5 h)	263.8	8.5	2.97
TiO_2(270 °C, 0.5 h)	255.4	9.0	2.79
TiO_2(300 °C, 0.5 h)	235.6	9.5	2.86
P-25	48.2	28.6	3.20

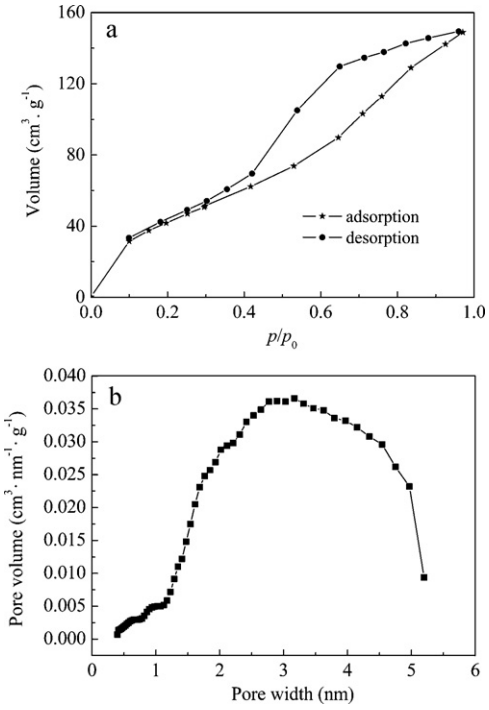

Fig. 3. Nitrogen adsorption–desorption isotherm (a) and DFT differential pore volume distribution (b) of TiO_2(270 °C, 0.5 h).

ferent time and of 8.2–9.5 nm (Table 2) for the samples heat-treated at different temperatures for 0.5 h. These results are in good agreement with the TEM results. With heat-treating time or temperature increasing, the mean size of TiO_2 nanoparticles slightly increases because of the growth of anatase crystals.

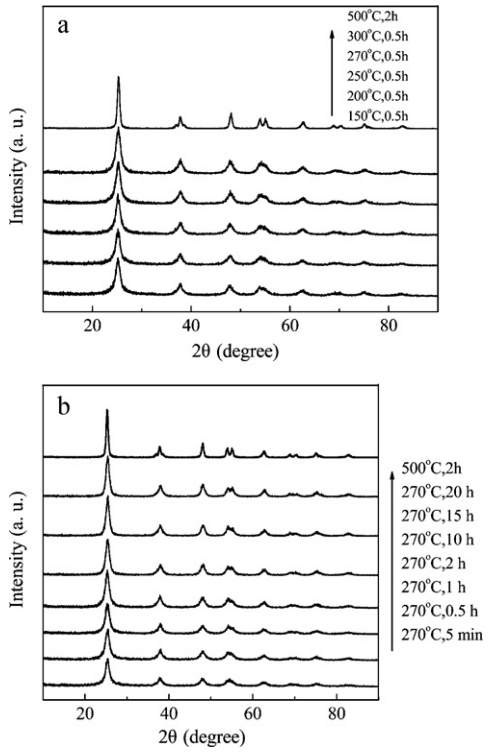

Fig. 4. XRD patterns of as-prepared TiO_2 heat-treated at different temperatures for 0.5 h (a) and heat-treated at 270 °C for different time (b).

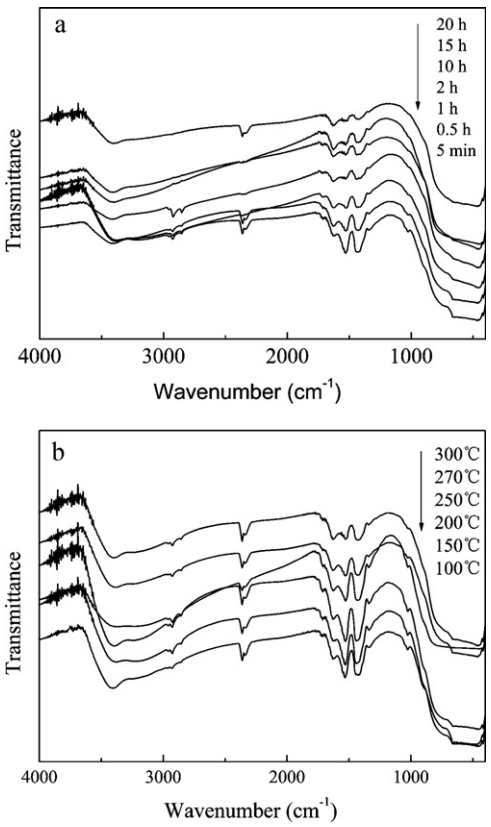

Fig. 5. FTIR spectra for as-prepared TiO_2 heat-treated at 270 °C for different time (a) and at different temperatures for 0.5 h (b).

3.1.3. FTIR and Raman spectra

Fig. 5(a) and (b) display FTIR spectra of the as-prepared TiO_2 heat-treated at 270 °C for different time and at different temperatures for 0.5 h, respectively. In the typical spectra of the investigated samples, there are some main characteristic peaks and they can be assigned as follows: the bands at 3387 cm^{-1} and 1530 cm^{-1} are assigned, respectively to the stretching and bending modes of hydroxyl group (–OH) or the adsorbed water on the TiO_2 surface. The band at 2363 cm^{-1} is assigned to CO_2 which comes from the environment. The band at 1630 cm^{-1} is assigned to C=C bond which comes from the butyl groups after the sample was heat-treated at the investigated temperatures. The bands at 2900–2800 cm^{-1} and 1430 cm^{-1} are corresponding to the stretching and bending modes of C–H bonds which come from the residual butyl group in the as-prepared TiO_2. The peak at 1073 cm^{-1} is corresponding to the stretching mode of C–O bond. The wide peak at 420–800 cm^{-1} corresponds to the Ti–O bending mode of TiO_2. The peak for the C=C bond intensifies while the peaks for the C–H bonds weaken simultaneously as the heat-treating time prolonging at 270 °C or the heat-treating temperature increasing for 0.5 h.

The curve (a) and curve (b) in Fig. 6 are the Raman spectra of commercial TiO_2 P-25 and TiO_2(270 °C, 0.5 h), respectively. The peaks at 145 cm^{-1}, 395 cm^{-1}, 515 cm^{-1} and 638 cm^{-1} in curve (a) are the characteristic ones of anatase TiO_2 [43]. The characteristic peaks for the as-prepared TiO_2 are at 152 cm^{-1}, 399 cm^{-1}, 519 cm^{-1} and 642 cm^{-1}, which move to higher wavenumbers by about 4 cm^{-1} compared with those for P-25. The peaks at 1590 cm^{-1} and 2940 cm^{-1} in curve (b) are assigned to C=C and C–H in the residual organic groups, respectively. The results further show that some organic groups exist in TiO_2 nanoparticles prepared at lower temperatures.

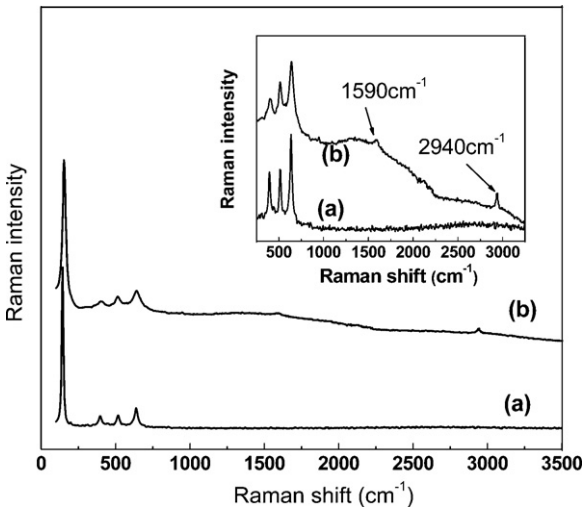

Fig. 6. Raman spectra of neat TiO_2 (a) and TiO_2(270 °C, 0.5 h) (b).

3.1.4. XPS

A typical XPS spectrum for TiO_2(270 °C, 0.5 h) is shown in Fig. 7(a). It can be found that TiO_2(270 °C, 0.5 h) only contains the elements of Ti, O and C, and the molar ratios of Ti, O and C are 16.3%, 47.9% and 35.8%, respectively. The binding energies of Ti $2p_{3/2}$, O 1s and C 1s are 458.3, 529.8 and 284.8 eV, respectively. The high content of C element comes from the residual organic groups in the as-prepared TiO_2 and the contaminated carbon from the environment. To understand the chemical state of C and O in the as-prepared TiO_2, the C 1s and O 1s core levels were measured as shown in Fig. 7(b) and (c). Three peaks can be observed at the binding energies of 284.6, 286.1 and 288.6 eV for C 1s, and three peaks at 529.7, 531.3 and 532.7 eV for O 1s. The peak of 284.6 eV reveals the presence of adventitious elemental carbon [44], the peak of 286.1 eV reveals the presence of C–C bonds in the residual organic groups, and the peak of 288.6 eV reveals the presence of C–O bonds [37], indicating that carbon atom might occupy the site of titanium atom to form a Ti–O–C structure [19]. The signal of O 1s at 529.7 eV confirms the Ti–O bond in TiO_2 and the other peaks at 531.3 and 532.7 eV may be attributed to the H-bonds between TiO_2 and the residual organic groups. Fig. 7(d) shows the XPS signals of Ti 2p. Two characteristic binding energies are found at 458.3 eV (Ti $2p_{3/2}$) and 464.5 eV (Ti $2p_{1/2}$), in good agreement with ordinary TiO_2. This finding further confirms that the titanium atom bonds with oxygen not carbon in the as-prepared TiO_2.

3.1.5. UV–vis DRS

Fig. 8(a) and (b) displays the UV–visible diffuse reflectance spectra of the as-prepared TiO_2 heat-treated at 270 °C for different time and at different temperatures for 0.5 h, respectively. It can be found that all the investigated as-prepared TiO_2 nanoparticles have higher absorbance in the visible light region than P-25, and with heat-treating time or temperature increasing, the absorbance of the as-prepared TiO_2 first increases and then decreases.

The band gap energies (E_g) of the as-prepared TiO_2 and P-25 can be obtained from the wavelength values corresponding to the intersection point of the vertical and horizontal parts of UV–vis DRS spectra using the equation: $hc/\lambda = Eg$, where, Eg is the band gap energy (eV), h the Planck's constant, c the light velocity (m/s), and λ the light wavelength (nm). The obtained band gap energies are shown in Tables 1 and 2. It can be found that the band gap energies of all the investigated as-prepared TiO_2 are obviously lower than that of P-25. With heat-treating time or temperature increasing, the band gap energies of the investigated as-prepared TiO_2 first decreases and then increases, similar to the absorbance in the visible light region.

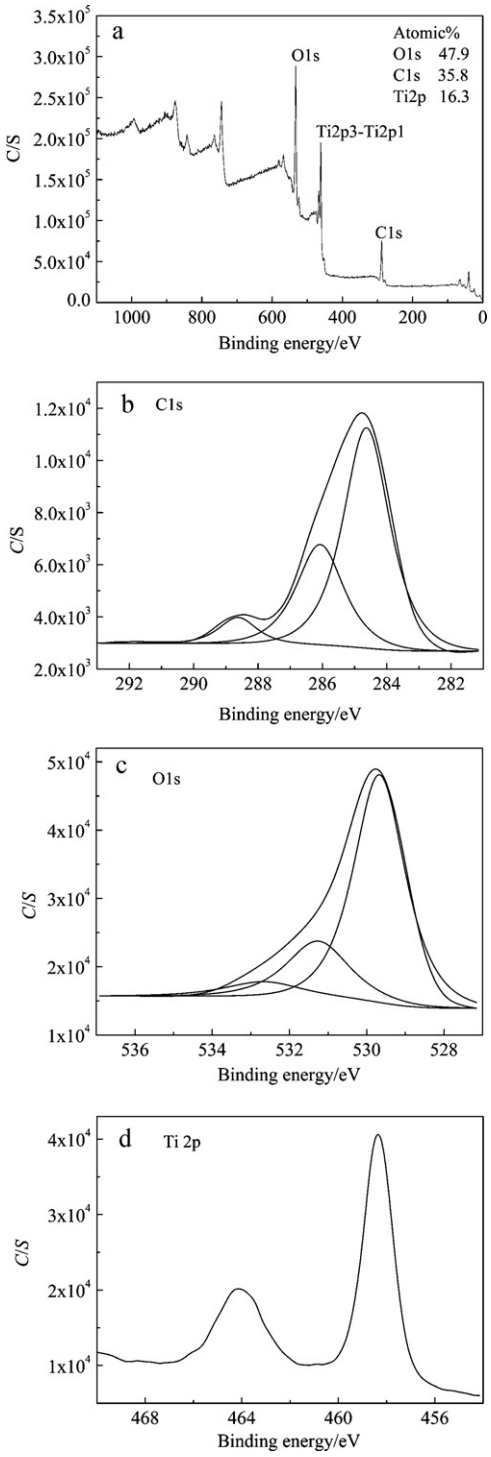

Fig. 7. XPS spectra of TiO_2(270 °C, 0.5 h): (a) survey spectrum, (b) C 1s, (c) O 1s and (d) Ti 2p.

The color of the as-prepared TiO_2 also changes with variations in the heat-treating temperature and time. With the increment of heat-treating time at 270 °C, the color of the investigated as-prepared TiO_2 gradually changes from white to brown, then from brown to yellow, until it finally becomes white. A similar result is obtained for the samples processed at different temperatures for 0.5 h. This phenomenon is related to the oxidation of the residual organic groups in the as-prepared TiO_2.

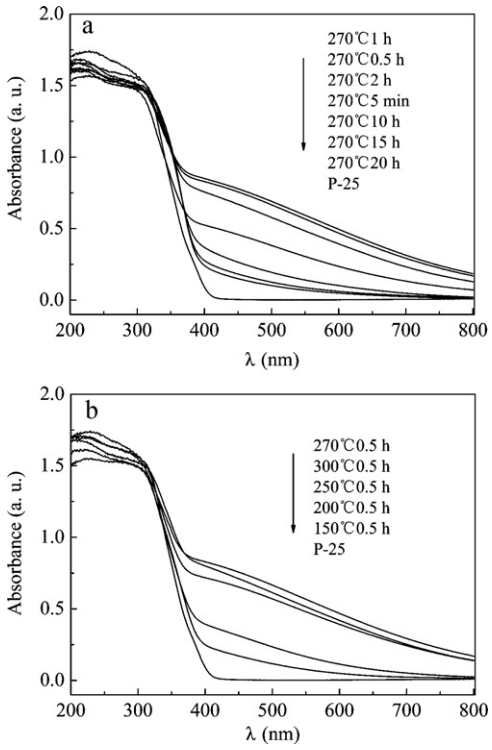

Fig. 8. UV–vis DRS spectra for as-prepared TiO_2 heat-treated at different time (a) and at different temperatures for 0.5 h (b).

3.1.6. DSC–TGA

The DSC–TGA curves of TiO_2(270 °C, 0.5 h) are presented in Fig. 9. Three weight loss regions appear in the TGA curve of the as-prepared TiO_2. The first weight loss of 5.5% occurring from 25 °C to 150 °C can be attributed to the desorption of the adsorbed water, the second weight loss of about 2.5% occurring from 150 °C to 300 °C can be attributed to the desorption of the crystal water and dehydrogenation of $–CH_2–CH_2–CH_2–CH_3$ in the as-prepared TiO_2, and the third weight loss of about 10.0% occurring from 300 °C to 620 °C may be attributed to the thermal decomposition of residual organic groups in the as-prepared TiO_2. In the DSC curve of the as-prepared TiO_2, the endothermic peak at about 60 °C is due to the loss of the adsorbed water and the endothermic peak at about 232 °C is related to the desorption of the crystal water and dehydrogenation of $–CH_2–CH_2–CH_2–CH_3$ in the as-prepared TiO_2, the peak at about 405 °C is due to the decomposition of the organic groups in the as-prepared TiO_2, and the peak at about 660 °C is attributed to the phase transformation of TiO_2 from anatase to rutile.

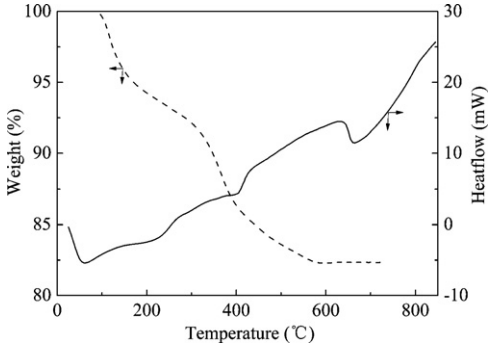

Fig. 9. DSC–TGA curves of TiO_2(270 °C, 0.5 h).

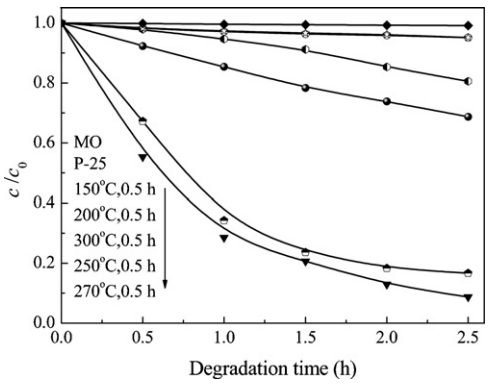

Fig. 10. The relationship between c/c_0 of MO and photodegradation time in the presence of as-prepared TiO_2 heat-treated at different temperatures for 0.5 h and TiO_2 (P-25) under visible light irradiation.

3.2. Visible light photocatalytic activity

The visible light photocatalytic activities of the as-prepared TiO_2 photocatalysts and reference sample P-25 were evaluated by the degradation of MO solutions. No degradation of MO was observed in the absence of a photocatalyst under visible light illumination. The MO concentration after the adsorption–desorption equilibrium in the presence of the as-prepared TiO_2 and P-25 decreased about 11% and 6.8%, respectively, and this MO adsorption on the photocatalyst was eliminated when the photocatalytic activities of the as-prepared TiO_2 and P-25 were evaluated. Fig. 10 shows the relationship between c/c_0 of MO and photodegradation time in the presence of P-25 and the as-prepared TiO_2 heat-treated at different temperatures for 0.5 h under visible light irradiation. It can be found that the photocatalytic activity of P-25 is the same as that of the sample TiO_2(150 °C, 0.5 h), while obviously lower than those of the other as-prepared TiO_2 samples, i.e., TiO_2(200 °C, 0.5 h), TiO_2(250 °C, 0.5 h), TiO_2(270 °C, 0.5 h) and TiO_2(300 °C, 0.5 h), revealing that these as-prepared TiO_2 samples possess higher visible light photocatalytic activity than P-25. The heat-treating temperature of the as-prepared TiO_2 greatly affects its visible light photocatalytic activity. With the heat-treating temperature increasing from 150 °C to 270 °C, the visible light photocatalytic activity of the as-prepared TiO_2 increases, and then begins to decrease at temperatures above 270 °C.

The relationships between c/c_0 of MO and photodegradation time in the presence of the as-prepared TiO_2 heat-treated at 270 °C for different time and P-25 are shown in Fig. 11. It is concluded that the photodegradation efficiency of MO for P-25 is obviously

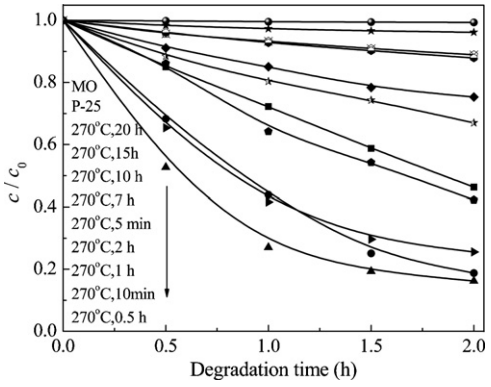

Fig. 11. The relationship between c/c_0 of MO and photodegradation time in the presence of as-prepared TiO_2 heat-treated at 270 °C for different time and TiO_2 (P-25) under visible light irradiation.

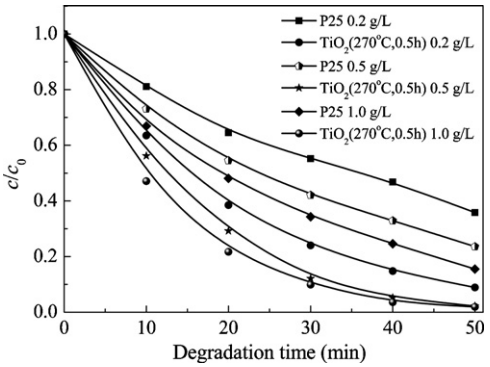

Fig. 12. Photodegradation of MO in the presence of TiO_2(270 °C, 0.5 h) and P-25 with different concentrations under solar light irradiation.

lower than those for all the investigated as-prepared TiO_2 samples, similarly revealing that the visible light photocatalytic activity of the as-prepared TiO_2 samples are higher than that of P-25. With the heat-treating time increasing, the visible light photocatalytic activity of the as-prepared TiO_2 dramatically increases and then gradually decreases. The TiO_2 nanoparticles show the best visible light photocatalytic activity at the heat-treating time of 0.5 h.

The photodegradation of MO in the presence of TiO_2(270 °C, 0.5 h) and P-25 at different photocatalyst concentrations (1 g L^{-1}, 0.5 g L^{-1} and 0.2 g L^{-1}) under sunlight irradiation is shown in Fig. 12. It can be found that the photocatalytic degradation rates of MO in the presence of TiO_2(270 °C, 0.5 h) at the investigated concentrations are much higher than those of P-25 under sunlight.

The MO photodegradations catalyzed by TiO_2(270 °C, 0.5 h) and other visible photocatalysts(such as PPy/TiO_2, PANI/TiO_2, P3HT/TiO_2 N–TiO_2 and Fe^{3+}–TiO_2) reported in literature [16,31–33,38] have been carried out under the same experimental conditions, and the comparative results on their visible light photocatalytic activities are shown in Fig. 13. It can be found that the visible light photocatalytic activity of TiO_2(270 °C, 0.5 h) is the best among those of the investigated photocatalysts.

To examine the photocatalytic stability, TiO_2(270 °C, 0.5 h) was chosen to carry out the recycling experiments and long time irradiation experiments under visible light. The regeneration of the TiO_2 photocatalyst in the recycling experiments was conducted by suspension filtration to remove the bulk solution and drying at 100 °C for 10 h, and then the regenerated TiO_2 was reused for the additional photocatalytic experiments. This process was repeated 10 times (Fig. 14). The visible light photocatalytic activity of TiO_2(270 °C, 0.5 h) irradiated under visible light for different time was tested in the long time irradiation experiments (Fig. 15). It can be found that the photodegradation efficiency of

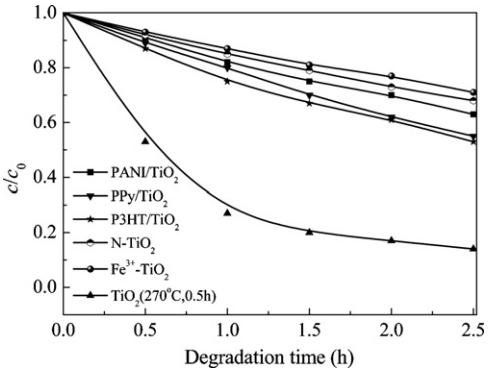

Fig. 13. MO photodegradation catalyzed by TiO_2(270 °C, 0.5 h), PPy/TiO_2, P3HT/TiO_2, PANI/TiO_2, N–TiO_2 and Fe^{3+}–TiO_2 under visible light irradiation.

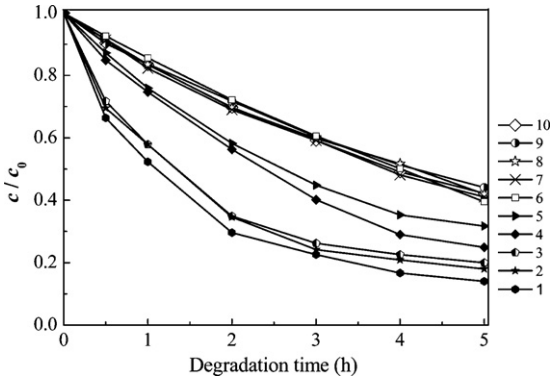

Fig. 14. Results of recycling experiment for TiO_2(270 °C, 0.5 h).

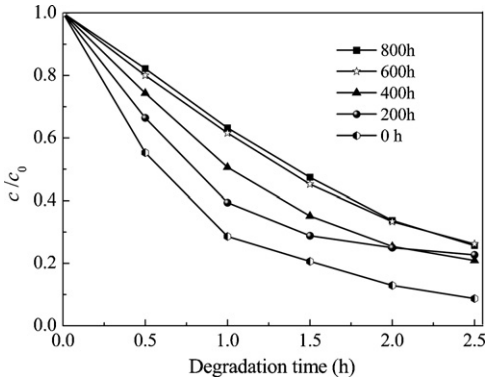

Fig. 15. Results of long time irradiation experiment under visible light for TiO_2(270 °C, 0.5 h).

MO slightly decreases with the recycling runs, and remains almost constant after five successive cycles, which is more than 70% of that of the first recycling run. The similar results are obtained from Fig. 15, in which the photodegradation efficiency of MO slightly decreases with the irradiation time under visible light, and is almost unchanged after 600 h of irradiation time for the investigated sample. The above results indicate that the as-prepared TiO_2 nanoparticles show excellent photocatalytic stability.

3.3. Discussion

During the preparation of TiO_2 gel by hydrolysis reaction of tetrabutyl titanate, some butyl groups would theoretically remain in the gel state of TiO_2 due to the incomplete hydrolysis of tetrabutyl titanate. The probable structure of the TiO_2 gel can be depicted in Scheme 1.

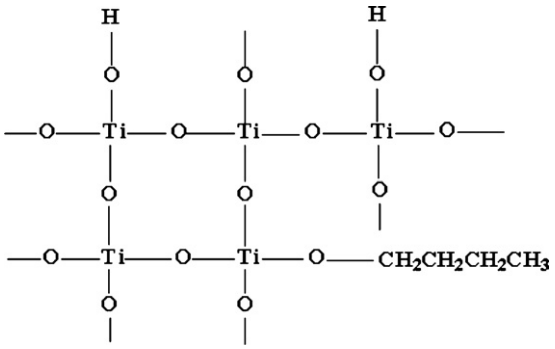

Scheme 1. The probable structure of TiO_2 gel.

Table 3
Apparent optical thickness, average LVRPA and kinetic constants k_T for as-prepared TiO_2 nanoparticles and P-25.

Samples	P-25	TiO_2(270 °C, 5 min)	TiO_2(270 °C, 0.5 h)	TiO_2(270 °C, 2 h)	TiO_2(270 °C, 10 h)
Incident radiation flux, I_0 (W m^{-2})	9.6	9.6	9.6	9.6	9.6
Thickness of suspension, δ (mm)	15	15	15	15	15
Extinction coefficient, $\sigma+\kappa$ (m^2 kg^{-1})	1168	1360	1503	1398	1248
Absorption coefficient, κ (m^2 kg^{-1})	8	200	343	238	88
Scattering albedo, ω	0.9932	0.8529	0.7718	0.8298	0.9295
Apparent optical thickness, τ_{app}	3.09	12.29	15.57	13.43	8.95
Absorbed radiant power, W_{abs} (W)	0.01118	0.03473	0.03919	0.03656	0.02840
Average LVRPA (W m^{-3})	116.4	361.8	408.3	380.9	295.9
k_{exp} (h^{-1})	0.0221	0.366	1.031	0.421	0.152
10^3 k_T (m^3 h^{-1} W^{-1})	0.1899	0.1012	0.2525	0.1105	0.5137

According to the structure of Ti–O–CH_2–CH_2–CH_2–CH_3 in Scheme 1, carbon atom in butyl group actually replaces Ti atom in TiO_2 to form some defects in the TiO_2 gel, which is a kind of carbon doping, i.e., carbon self-doping. When the TiO_2 gel is heat-treated at the investigated temperatures, a series of complex reactions can take place for the butyl groups in TiO_2 to form the carbonaceous residue. Therefore, the characteristic results of FTIR, Raman and XPS clearly show the evidence of carbonaceous residue or elemental carbon and not butyl groups, confirming the conclusion of carbon self-doping. Similarly results were obtained by Park et al., who also reported that TiO_2 prepared at lower temperatures (≤300 °C) possesses a carbon self-doping structure [37]. TiO_2 with this carbon self-doping structure exhibits visible light photocatalytic activity. Therefore, carbon self-doping in the as-prepared TiO_2 may be one of the reasons for enhancing its visible light photocatalytic activity.

In the heat-treating process of the as-prepared TiO_2, the bond of C–O in the Ti–O–CH_2–CH_2–CH_2–CH_3 group can be broken. The increment of heat-treating temperature or time can be favorable to the O–C bond breakage, leading to the improved crystallinity and size of TiO_2 crystals and decreased specific surface area of TiO_2 nanoparticles, which can be supported by the results of XRD and N_2 sorption analysis. Meanwhile, other reactions, such as the dehydrogenation of n-butyl group –CH_2–CH_2–CH_2–CH_3 in the presence of TiO_2, could also occur at the investigated processing temperatures. If the dehydrogenation of –CH_2–CH_2–CH_2–CH_3 exactly occurs, the dehydrogenated groups from –CH_2–CH_2–CH_2–CH_3 may be the visible light sensitive groups, such as the groups containing the double bond –CH=CH–. The results of FTIR and Raman reveal that the double bond –CH=CH– exists in the as-prepared TiO_2. The as-prepared TiO_2 containing the photosensitive organic groups can easily absorb and be excited by visible light to generate the electron/hole pairs. Therefore, the photosensitization of the photosensitive organic groups on the surface of the as-prepared TiO_2 may be another major reason for enhancing its visible light photocatalytic activity.

The actual photocatalytic activity of the as-prepared TiO_2 under visible light irradiation depends on the combined effects of the above two factors, i.e., carbon self-doping and visible photosensitive groups in the as-prepared TiO_2. The increment of the amount of the visible light photosensitive groups is favorable to the visible light photocatalytic activity of the as-prepared TiO_2, whereas the decrement of the degree of carbon self-doping and amount of visible light photosensitive groups is unfavorable. When the heat-treating temperature increases from 150 °C to 270 °C, the content of visible light photosensitive groups in the as-prepared TiO_2 obviously increases because the dehydrogenation of –CH_2–CH_2–CH_2–CH_3 can more easily occur in the presence of TiO_2 (the color of the as-prepared TiO_2 dramatically changes from white to deep), while the degree of carbon self-doping, crystal crystallinity and specific surface area slightly change because of the difficulty of the C–O bond breakage in the range of investigated temperatures. The increment of the content of visible light photosensitive groups is the major factor affecting the visible light photocatalytic activity. Therefore, the visible light photocatalytic activity of the as-prepared TiO_2 increases. However, when the heat-treating temperature increases from 270 °C to 300 °C, the breakage of C–O bond in Ti–O–CH_2–CH_2–CH_2–CH_3 can easily occur and gradually becomes the major reaction, leading to a considerable decrement of the degree of carbon self-doping and amount of visible light photosensitive groups (The color of the as-prepared TiO_2 changes from deep to light), thus, the visible light photocatalytic activity of the as-prepared TiO_2 decreases. If the heat-treating temperature is over 400 °C, the structure of Ti–O–C hardly exists in TiO_2 nanoparticles because of the breakage of the C–O bond. Both carbon self-doping and visible light photosensitive groups disappear, so that the visible light photocatalytic activity of TiO_2 prepared at higher temperature (≥400 °C) is very low.

The effect of heat-treating time on the visible light photocatalytic activity of the as-prepared TiO_2 is similar to that of heat-treating temperatures. When the heat-treating time increases from 5 min to 0.5 h, the amount of visible light photosensitive groups visibly increases, whereas the other factors do not greatly change. Therefore, the increment in the amount of visible light photosensitive groups is the major factor affecting the visible light photocatalytic activity of the as-prepared TiO_2, leading to the increased visible light photocatalytic activity. When the heat-treating time increases from 0.5 h to 15 h, the breakage of the C–O bond in Ti–O–CH_2–CH_2–CH_2–CH_3 gradually becomes the major reaction while the dehydrogenation of –CH_2–CH_2–CH_2–CH_3 slows down, the degree of carbon self-doping and amount of visible light photosensitive groups dramatically decreases, leading to the decrement of the visible light photocatalytic activity of the as-prepared TiO_2. When the heat-treating time is more than 15 h, both the breakage of the C–O bond and the dehydrogenation hardly occur, and all the affecting factors change little, thus, the visible light photocatalytic activity of the as-prepared TiO_2 barely changes.

The photodegradation system investigated in this work is a typical slurry suspension. According to the theory and calculation method described in literature [39–41], we chose four as-prepared TiO_2 samples (TiO_2(270 °C, 5 min), TiO_2(270 °C, 0.5 h), TiO_2(270 °C, 2 h) and TiO_2(270 °C, 10 h)) and P-25 to determine the apparent optical thickness (τ_{app}), which is a dimensionless and important parameter for designing the photodegradation reactor. To calculate τ_{app}, the extinction coefficient ($\sigma+\kappa$) and absorption coefficient (κ) of the as-prepared TiO_2 must be known. The two parameters can be obtained by the method reported in literature [45]. The values of extinction coefficient, absorption coefficient and apparent optical thickness are listed in Table 3. It can be found from Table 3 that the values of τ_{app} for the as-prepared TiO_2 are in the range of those reported in literature [41], and much higher than that for P-25.

The local volumetric rate of photon absorption (LVRPA) is another important parameter for the photoreaction, which can be used to estimate the photodegradation kinetics according to the following equation:

$$R = k_T(\text{LVRPA})^m c^n$$

Table 4
Apparent optical thickness, average LVRPA and kinetic constants k_T for TiO_2 (270 °C, 0.5 h) and the other visible photocatalysts reported in literature.

Samples	TiO_2(270 °C, 0.5 h)	TiO_2/PANI	TiO_2/PPy	TiO_2/P3TH	N–TiO_2	Fe^{3+}–TiO_2
Incident radiation flux, I_0 (W m^{-2})	9.6	9.6	9.6	9.6	9.6	9.6
Thickness of suspension, δ (mm)	15	15	15	15	15	15
Extinction coefficient, $\sigma+\kappa$ (m^2 kg^{-1})	1503	1302	1315	1321	1294	1286
Absorption coefficient, κ (m^2 kg^{-1})	343	142	155	161	134	126
Scattering albedo, ω	0.7718	0.8909	0.8821	0.8781	0.8964	0.9020
Apparent optical thickness, τ_{app}	15.57	10.86	11.25	11.43	10.61	10.35
Absorbed power, W_{abs} (W)	0.03919	0.03248	0.03316	0.03346	0.03202	0.03153
Average LVRPA (W m^{-3})	408.3	338.3	345.5	348.6	333.6	328.5
k_{exp} (h^{-1})	1.031	0.185	0.238	0.257	0.156	0.136
$10^3 k_T$ (m^3 h^{-1} W^{-1})	2.525	0.5469	0.6889	0.7372	0.4676	0.4141

Table 5
Apparent optical thickness, average LVRPA and kinetic constants k_T for TiO_2 (270 °C, 0.5 h) and P-25 under solar radiation.

Samples	TiO_2(270 °C, 0.5 h)	P-25	TiO_2(270 °C, 0.5 h)	P-25	TiO_2(270 °C, 0.5 h)	P-25
Concentration of TiO_2 (kg m^{-3})	1.0	1.0	0.5	0.5	0.2	0.2
Incident radiation flux, I_0 (W m^{-2})	26	26	26	26	26	26
Thickness of suspension, δ (mm)	15	15	15	15	15	15
Extinction coefficient, $\sigma+\kappa$ (m^2 kg^{-1})	1808	1470	1808	1470	1808	1470
Absorption coefficient, κ (m^2 kg^{-1})	518	180	518	180	518	180
Scattering albedo, ω	0.7135	0.8776	0.7135	0.8776	0.7135	0.8776
Apparent optical thickness, τ_{app}	27.12	22.05	13.56	11.02	5.42	4.41
Absorbed power, W_{abs} (W)	0.1136	0.0907	0.1134	0.0905	0.1115	0.0808
Average LVRPA (W m^{-3})	1183	945	1183	944	1163	842
k_{exp} (h^{-1})	4.782	2.184	4.392	1.722	2.874	1.206
$10^3 k_T$ (m^3 h^{-1} W^{-1})	4.042	2.311	3.713	1.824	2.471	1.432

where k_T is the kinetic constant, c is the concentration of the photodegraded compound, m and n are the reaction orders with respect to the average LVRPA and c, respectively. The average values of LVRPA, calculated by the method reported in literature [39–41], are listed in Table 3. The relationship between $\ln(c_0/c)$ and reaction time (not shown here) shows that the MO photodegradation catalyzed by the as-prepared TiO_2 and P-25 is the first-order reaction, and the apparent rate constant k_{exp} can be obtained from this relationship (Table 3). On the basis of the reported results [40,41], we can suppose that $m = 1.0$ to estimate the value of k_T from $k_{exp} = k_T$(LVRPA) (Table 3). It can be found that the values of k_T for the as-prepared TiO_2 are greatly higher than that for P-25, indicating that the separation efficiency of photogenerated electrons and holes for the as-prepared TiO_2 may be higher than that for P-25.

Similarly, the values of τ_{app}, average LVRPA and k_T for TiO_2(270 °C, 0.5 h) and the other visible photocatalysts (P3HT/TiO_2, PANI/TiO_2, PPy/TiO_2, N–TiO_2 and Fe^{3+}–TiO_2) under visible light irradiation were calculated and listed in Table 4. It can be found that the values of τ_{app} are in the same range as those reported in literature [40], and the value of k_T for TiO_2(270 °C, 0.5 h) under visible light irradiation is the highest among those of the investigated samples, further revealing that TiO_2(270 °C, 0.5 h) is one of excellent visible photocatalysts.

The solar light includes UV and visible light, so the absorption coefficients (κ) for TiO_2(270 °C, 0.5 h) and P-25 under solar light are much higher than the corresponding values under visible light (Table 5). According to literature [40,41], the values of τ_{app}, average LVRPA and k_T for TiO_2(270 °C, 0.5 h) and P-25 at different concentrations (1 g L^{-1}, 0.5 g L^{-1} and 0.2 g L^{-1}) under solar light irradiation were calculated and listed in Table 5. Table 5 shows that the values of τ_{app} dramatically decrease with the decrement of photocatalyst concentration, and are in the same range as those reported in literature [40] at the photocatalyst concentration of about 0.5 g L^{-1}, indicating that the optimal photocatalyst concentration could be 0.5 g L^{-1} under solar light irradiation. The values of k_T for TiO_2(270 °C, 0.5 h) are still much higher than those for P-25, but the improving degree (about twofold) is obviously less than that (about 13-fold) under visible light irradiation because P-25 can absorb UV light under solar light irradiation. Therefore, TiO_2(270 °C, 0.5 h) is a promising photocatalyst candidate under visible and solar light.

4. Conclusions

Highly efficient visible light TiO_2 photocatalyst was prepared by the sol–gel method at lower temperatures (≤300 °C) with tetrabutyl titanate, ethanol absolute and acetic acid glacial as the major feeds, and characterized by XRD, TEM, FTIR, UV–vis DRS, XPS, Raman Spectra and DSC–TGA. Results show the as-prepared TiO_2 nanoparticles possess an anatase phase and mesoporous structure with carbon self-doping and visible photosensitive organic groups. The visible light photocatalytic activity of the as-prepared TiO_2 is greatly higher than those of the commercial TiO_2 (P-25) and other visible photocatalysts (such as PPy/TiO_2, PANI/TiO_2, P3HT/TiO_2, N–TiO_2 and Fe^{3+}–TiO_2) reported in literature, and its photocatalytic stability is excellent. The heat-treating temperature or time obviously affects the visible light photocatalytic activity of the as-prepared TiO_2. With the increment of the heat-treating temperature or time, the visible light photocatalytic activity increases and then decreases. The improvement in the visible light photocatalytic activity of the as-prepared TiO_2 can be attributed to carbon self-doping and photosensitization of the visible photosensitive organic groups existing in the as-prepared TiO_2. The changes in the visible light photocatalytic activity of the as-prepared TiO_2 with the heat-treating temperature or time can be explained by the combined effects of carbon self-doping and photosensitization of the visible photosensitive groups on its visible light photocatalytic activity. TiO_2(270 °C, 0.5 h) can be an excellent photocatalyst candidate for the degradation of the organic contaminants under visible and solar light irradiation.

Acknowledgments

The authors are grateful for the financial support by the National Natural Science Foundation of China (51002044) and the Nat-

ural Science Foundation of Hebei Province (B2010000846 and B2011208006).

References

[1] A.D. Paola, G. Cufalo, M. Addamo, M. Bellardita, R. Campostrini, M. Ischia, R. Ceccato, L. Palmisano, Photocatalytic activity of nanocrystalline TiO_2 (brookite, rutile and brookite-based) powders prepared by thermohydrolysisof $TiCl_4$ in aqueous chloride solutions, Colloid Surf. A 317 (2008) 366–376.

[2] A. Bendavid, P.J. Martin, Å. Jamting, H. Takikawa, Structural and optical properties of titanium oxide thin films deposited by filtered arc deposition, Thin Solid Films 355–356 (1999) 6–11.

[3] Y. Ku, R.M. Leu, K.C. Lee, Decomposition of 2-chlorophenol in aqueous solution by UV irradiation with the presence of titanium dioxide, Water Res. 30 (1996) 2569–2578.

[4] V.N.H. Nguyen, R. Amal, D. Beydoun, Effect of formate and methanol on photoreduction/removal of toxic cadmium ions using TiO_2 semiconductor as photocatalyst, Chem. Eng. Sci. 58 (2003) 4429–4439.

[5] C. Kormann, D.W. Bahnemann, M.R. Hoffmann, Preparation and characterization of quantum-size titanium dioxide, J. Phys. Chem. 92 (1988) 5196–5201.

[6] G. Cao, Y. Li, Q. Zhang, H. Wang, Synthesis and characterization of $La_2O_3/TiO_{2-x}F_x$ and the visible light photocatalytic oxidation of 4-chlorophenol, J. Hazard. Mater. 178 (2010) 440–449.

[7] S. Kaur, V. Singh, Visible light induced sonophotocatalytic degradation of Reactive Red dye 198 using dye sensitized TiO_2, Ultrason. Sonochem. 14 (2007) 531–537.

[8] D. Chatterjee, S. Dasgupta, N.N. Rao, Visible light assisted photodegradation of halocarbons on the dye modified TiO_2 surface using visible light, Sol. Energy Mater. Sol. Cells 90 (2006) 1013–1020.

[9] K.S. Yao, T.C. Cheng, S.J. Li, L.Y. Yang, K.C. Tzeng, C.Y. Chang, Y. Ko, Comparison of photocatalytic activities of various dye-modified TiO_2 thin films under visible light, Surf. Coat. Technol. 203 (2008) 922–924.

[10] D. Jiang, Y. Xu, D. Wu, Y. Sun, Visible-light responsive dye-modified TiO_2 photocatalyst, J. Solid State Chem. 181 (2008) 593–602.

[11] G. Liu, X. Zhang, Y. Xu, X. Niu, L. Zheng, X. Ding, The preparation of Zn^{2+}-doped TiO_2 nanoparticles by sol–gel and solid phase reaction methods, respectively and their photocatalytic activities, Chemosphere 59 (2005) 1367–1371.

[12] L. Sun, J. Li, C.L. Wang, S.F. Li, H.B. Chen, C.J. Lin, An electrochemical strategy of doping Fe^{3+} into TiO_2 nanotube array films for enhancement in photocatalytic activity, Sol. Energy Mater. Sol. Cells 93 (2009) 1875–1880.

[13] M. Asiltürk, F. Sayılkana, E. Arpac, Effect of Fe^{3+} ion doping to TiO_2 on the photocatalytic degradation of Malachite Green dye under UV and vis-irradiation, J. Photochem. Photobiol. A: Chem. 203 (2009) 64–71.

[14] L. Kumaresan, M. Mahalakshmi, M. Palanichamy, V. Murugesan, Synthesis, characterization, and photocatalytic activity of Sr^{2+} doped TiO_2 nanoplates, Ind. Eng. Chem. Res. 49 (2010) 1480–1485.

[15] R. Asahi, T. Morikawa, T. Ohwaki, K. Aoki, Y. Taga, Visible-light photocatalysis in nitrogen-doped titanium oxides, Science 293 (2001) 269–271.

[16] J. Ananpattarachai, P. Kajitvichyanukul, S. Seraphin, Visible light absorption ability and photocatalytic oxidation activity of various interstitial N-doped TiO_2 prepared from different nitrogen dopants, J. Hazard. Mater. 168 (2009) 253–261.

[17] S. Yang, H. Hu, Y. Chen, J. Zheng, Y. Cui, Role of the reduction site in the fluorinated or sulfated TiO_2 photocatalytic process, J. Environ. Sci. 19 (2007) 1239–1244.

[18] M. Janus, M. Inagaki, B. Tryba, M. Toyoda, A.W. Morawski, Carbon-modified TiO_2 photocatalyst by ethanol carbonization, Appl. Catal. B: Environ. 63 (2006) 272–276.

[19] W. Ren, Z. Ai, F. Jia, L. Zhang, X. Fan, Z. Zou, Low temperature preparation and visible light photocatalytic activity of mesoporous carbon-doped crystalline TiO_2, Appl. Catal. B: Environ. 69 (2007) 138–144.

[20] H. Tian, J. Ma, K. Li, J. Li, Hydrothermal synthesis of S-doped TiO_2 nanoparticles and their photocatalytic ability for degradation of methyl orange, Ceram. Int. 35 (2009) 1289–1292.

[21] X. Hong, Z. Wang, W. Cai, F. Lu, J. Zhang, Y. Yang, N. Ma, Y. Liu, Visible-light-activated nanoparticle photocatalyst of iodine-doped titanium dioxide, Chem. Mater. 17 (2005) 1548–1552.

[22] X.G. Hou, F.H. Hao, B. Fan, X.N. Gu, X.Y. Wu, A.D. Liu, Modification of TiO_2 photocatalytic films by V^+ ion implantation, Nucl. Instrum. Method Phys. Res. B 243 (2006) 99–102.

[23] M.C. Hidalgo, M. Maicu, J.A. Navío, G. Colón, Effect of sulfate pretreatment on gold-modified TiO_2 for photocatalytic applications, J. Phys. Chem. C 113 (2009) 12840–12847.

[24] H.M. Sung-Suh, J.R. Choi, H.J. Hah, S.M. Koo, Y.C. Bae, Comparison of Ag deposition effects on the photocatalytic activity of nanoparticulate TiO_2 under visible and UV light irradiation, J. Photochem. Photobiol. A: Chem. 163 (2004) 37–44.

[25] C.C. Chan, C.C. Chang, W.C. Hsu, S.K. Wang, J. Lin, Photocatalytic activities of Pd-loaded mesoporous TiO_2 thin films, Chem. Eng. J. 152 (2009) 492–497.

[26] S. Anandan, P. Sathish Kumar, N. Pugazhenthiran, J. Madhavan, P. Maruthamuthu, Effect of loaded silver nanoparticles on TiO_2 for photocatalytic degradation of Acid Red 88, Sol. Energy Mater. Sol. Cells 92 (2008) 929–937.

[27] J. Zhang, H. Zhu, S. Zheng, F. Pan, T. Wang, TiO_2 film/Cu_2O microgrid heterojunction with photocatalytic activity under solar light irradiation, ACS Appl. Mater. Interfaces 10 (2009) 2111–2114.

[28] J.Y. Kim, C.S. Kim, H.K. Chang, T.O. Kim, Effects of ZrO_2 addition on phase stability and photocatalytic activity of ZrO_2/TiO_2 nanoparticles, Adv. Powder Technol. 21 (2010) 141–144.

[29] M. Zhou, J. Yu, S. Liu, P. Zhai, L. Jiang, Effects of calcination temperatures on photocatalytic activity of SnO_2/TiO_2 composite films prepared by an EPD method, J. Hazard. Mater. 154 (2008) 1141–1148.

[30] M. Bellardita, M. Addamo, A.D. Paola, G. Marcì, L. Palmisano, L. Cassar, M. Borsa, Photocatalytic activity of TiO_2/SiO_2 systems, J. Hazard. Mater. 174 (2010) 707–713.

[31] D. Wang, J. Zhang, Q. Luo, X. Li, Y. Duan, J. An, Characterization and photocatalytic activity of poly(3-hexylthiophene)-modified TiO_2 for degradation of methyl orange under visible light, J. Hazard. Mater. 169 (2009) 546–550.

[32] X. Li, D. Wang, G. Cheng, Q. Luo, J. An, Y. Wang, Preparation of polyaniline-modified TiO_2 nanoparticles and their photocatalytic activity under visible light illumination, Appl. Catal. B: Environ. 81 (2008) 267–273.

[33] D. Wang, Y. Wang, X. Li, Q. Luo, J. An, J. Yue, Sunlight photocatalytic activity of polypyrrole–TiO_2 nanocomposites prepared by 'in situ' method, Catal. Commun. 9 (2008) 1162–1166.

[34] Q. Tang, J. Lin, Z. Wu, J. Wu, M. Huang, Y. Yang, Preparation and photocatalytic degradability of TiO_2/polyacrylamide composite, Eur. Polym. J. 43 (2007) 2214–2220.

[35] J. Wang, J. Yu, Z. Liu, Z. He, R. Cai, A simple new way to prepare anatase TiO_2 hydrosol with high photocatalytic activity, Semicond. Sci. Technol. 20 (2005) L36–L39.

[36] Y.H. Tseng, C.S. Kuo, C.H. Huang, Y.Y. Li, P.W. Chou, C.L. Cheng, M.S. Wong, Visible-light-responsive nano-TiO_2 with mixed crystal lattice and its photocatalytic activity, Nanotechnology 17 (2006) 2490–2497.

[37] Y. Park, W. Kim, H. Park, T. Tachikawa, T. Majima, W. Choi, Carbon-doped TiO_2 photocatalyst synthesized without using an external carbon precursor and the visible light activity, Appl. Catal. B: Environ. 91 (2009) 355–361.

[38] T. Tong, J. Zhang, B. Tian, F. Chen, D. He, Preparation of Fe^{3+}-doped TiO_2 catalysts by controlled hydrolysis of titanium alkoxide and study on their photocatalytic activity for methyl orange degradation, J. Hazard. Mater. 155 (2008) 572–579.

[39] G. Li Puma, A. Brucato, Dimensionless analysis of slurry photocatalytic reactors using two-flux and six flux radiation absorption–scattering models, Catal. Today 122 (2007) 78–90.

[40] J. Colina-Marquez, F. Machuca-martinez, G. Li Puma, Radiation absorption and optimization of solar photocatalytic reactors for environmental applications, Environ. Sci. Technol. 44 (2010) 5112–5120.

[41] J. Colina-Marquez, F. Machuca-martinez, G. Li Puma, Photocatalytic mineralization of commercial herbicides in a pilot-scale solar CPC reactor: photoreactor modeling and reaction kinetics constants independent of radiation field, Environ. Sci. Technol. 43 (2009) 8953–8960.

[42] K.S.W. Sing, D.H. Everett, R.A.W. Haul, L. Moscou, R.A. Pierotti, J. Rouquerol, T. Siemieniewska, Reporting physisorption data for gas/solid systems with special reference to the determination of surface area and porosity, Pure Appl. Chem. 57 (1985) 603–619.

[43] S. Orlanducci, V. Sessa, M.L. Terranova, G.A. Battiston, S. Battiston, R. Gerbasi, Nanocrystalline TiO_2 on single walled carbon nanotube arrays: towards the assembly of organized C/TiO_2 nanosystems, Carbon 44 (2006) 2839–2843.

[44] Y. Li, D.S. Hwang, N.H. Lee, S.J. Kim, Synthesis and characterization of carbon-doped titania as an artificial solar light sensitive photocatalyst, Chem. Phys. Lett. 404 (2005) 25–29.

[45] M.I. Cabrera, O.M. Alfano, A.E. Cassano, Absorption and scattering coefficients of titanium dioxide particulate suspensions in water, J. Phys. Chem. 100 (1996) 20043–20050.